

# Ultrafast glutamate sensors resolve high-frequency release at Schaffer collateral synapses

Nordine Helassa<sup>1</sup>, Celine Durst<sup>2</sup>, Catherine Coates<sup>1</sup>, Silke Kerruth<sup>1</sup>, Urwa Arif<sup>1</sup>, Christian Schulze<sup>2</sup>, J. Simon Wiegert<sup>2</sup>, Michael Geeves<sup>3</sup>, Thomas Oertner<sup>2</sup>, Katalin Torok<sup>1</sup>

<sup>1</sup>St George's, University of London, <sup>2</sup>Center for Molecular Neurobiology Hamburg, <sup>3</sup>University of Kent

Submitted to Proceedings of the National Academy of Sciences of the United States of America

**Glutamatergic synapses display a rich repertoire of plasticity mechanisms on many different time scales, involving dynamic changes in the efficacy of transmitter release as well as changes in the number and function of postsynaptic glutamate receptors. The genetically encoded glutamate sensor iGluSnFR enables visualization of glutamate release from presynaptic terminals at frequencies up to ~10 Hz. However, to resolve glutamate dynamics during high frequency bursts, faster indicators are required. Here we report the development of fast (iGlu<sub>f</sub>) and ultrafast (iGlu<sub>u</sub>) variants with comparable brightness, but increased  $K_d$  for glutamate (137  $\mu$ M and 600  $\mu$ M, respectively). Compared to iGluSnFR, iGlu<sub>u</sub> has a 6-fold faster dissociation rate *in vitro* and 5-fold faster kinetics in synapses. Fitting a three-state model to kinetic data, we identify the large conformational change after glutamate binding as the rate-limiting step. In rat hippocampal slice culture stimulated at 100 Hz, we find that iGlu<sub>u</sub> is sufficiently fast to resolve individual glutamate release events, revealing that glutamate is rapidly cleared from the synaptic cleft. Depression of iGlu<sub>u</sub> responses during 100 Hz trains correlates with depression of postsynaptic EPSPs, indicating that depression during high frequency stimulation is purely presynaptic in origin. At individual boutons, the recovery from depression could be predicted from the amount of glutamate released on the second pulse (paired pulse facilitation/depression), demonstrating differential frequency-dependent filtering of spike trains at Schaffer collateral boutons.**

glutamate | synaptic transmission | post-tetanic potentiation | hippocampus | two-photon imaging

## Introduction

The efficacy of synaptic transmission is not constant, but changes dynamically during high-frequency activity. In terms of information processing, different forms of short-term plasticity act as specific frequency filters: facilitating synapses are most effective during high frequency bursts, while depressing synapses preferentially transmit isolated spikes preceded by silent periods (1). Mechanistically, a number of pre- and postsynaptic parameters change dynamically during high frequency activity, e.g. the number of readily releasable vesicles, presynaptic  $Ca^{2+}$  dynamics, and the properties of postsynaptic receptors, which may be altered by  $Ca^{2+}$ -activated enzymes (2, 3).

Electrophysiological analysis of short-term plasticity, by monitoring postsynaptic responses, is complicated by the fact that neurons are often connected by more than one synapse. In addition, it is not straightforward to distinguish between pre- and postsynaptic plasticity mechanisms. Directly measuring glutamate concentrations inside the synaptic cleft during high-frequency activity would allow isolating the dynamics of the vesicle release machinery from potential changes in glutamate receptor properties (e.g. desensitization, phosphorylation or lateral diffusion). Early fluorescent glutamate sensors, constructed by chemical labelling of the fused glutamate binding lobes of ionotropic glutamate receptor GluA2 (termed S1S2) (4-6) and later of the bacterial periplasmic glutamate/aspartate binding protein (GluBP) (7, 8), were not suitable for quantitative single-synapse experiments due

to their low dynamic range. Genetically encoded FRET-based fluorescent glutamate sensors e.g. FLIPE, GluSnFR and Super-GluSnFR (Fig. 1a) have relatively low FRET efficiency, since glutamate binding causes only a small conformational change in GluBP (9-11). A breakthrough in visualizing glutamate release in intact tissue was achieved with iGluSnFR, a single-fluorophore glutamate sensor (12). Following the concept developed for the GCaMP family of genetically encoded  $Ca^{2+}$  sensors (13), iGluSnFR was constructed from circularly permuted (cp) EGFP (14) inserted into the GluBP sequence, creating a large fragment iGlu<sub>l</sub> (residues 1-253) at the N-terminus and a small fragment iGlu<sub>s</sub> (residues 254-279) at the C-terminus (Fig. 1a). Upon glutamate binding GluBP is reconstituted from its two fragments, pulling the cpEGFP  $\beta$ -barrel together, resulting in a ~5-fold fluorescence increase. iGluSnFR is targeted for extracellular expression, like previous genetically encoded glutamate sensors, by fusion with a PDGFR peptide segment (10, 12).

iGluSnFR has high glutamate affinity and a large dynamic range, but reacts relatively slowly to synaptic glutamate release with a reported decay half-time ( $t_{1/2}$ ) of 92 ms (12). Imaging iGluSnFR in cultured hippocampal neurons during 10 Hz stimulation shows summation, which, without deconvolution, might indicate that glutamate accumulates during stimulation (15). Deconvolution of the data suggests that glutamate is cleared between release events (15). Here we introduce two fast iGluSnFR variants, iGlu<sub>f</sub> (for 'fast') and iGlu<sub>u</sub> (for 'ultrafast') for accurate tracking of synaptic glutamate dynamics during high frequency transmission and identify the rate-limiting step leading to bright fluorescence upon glutamate binding. In organotypic

## Significance

**Excitatory synapses convert presynaptic action potentials into chemical signals that are sensed by postsynaptic glutamate receptors. To eavesdrop on synaptic transmission, genetically encoded fluorescent sensors for glutamate have been developed. However, even the best available sensors lag behind the very fast glutamate dynamics in the synaptic cleft. Here we report the development of an ultrafast genetically encoded glutamate sensor, iGlu<sub>u</sub>, which allowed us to image glutamate clearance and synaptic depression during 100 Hz spike trains. We found that only boutons showing paired-pulse facilitation were able to rapidly recover from depression. Thus, presynaptic boutons act as frequency-specific filters to transmit select features of the spike train to specific postsynaptic cells.**

## Reserved for Publication Footnotes

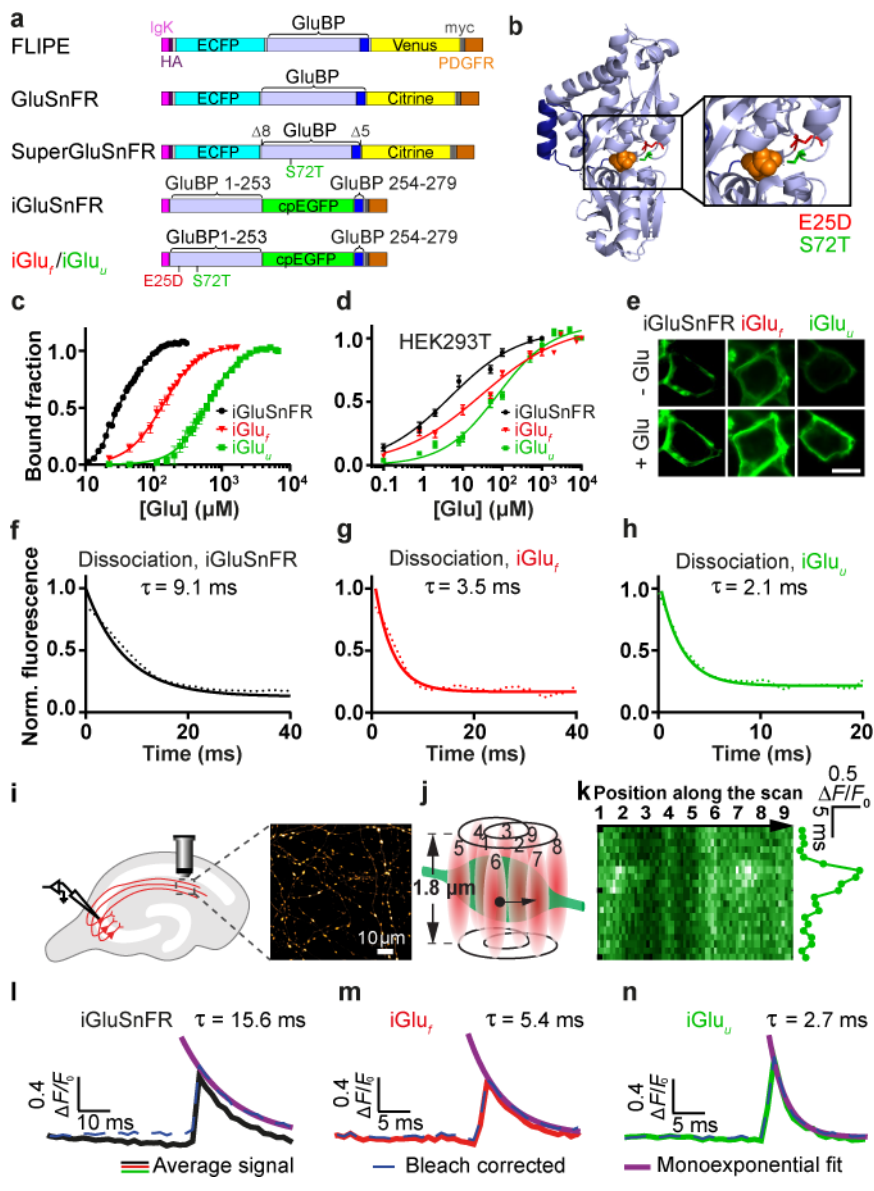


**Fig. 1.** Genetically encoded glutamate indicators (GEGI). (a) Domain structure and design of FRET- and single fluorophore-based GEGI; key: (GluBP) (blue), cpEGFP (green), IgG kappa secretion tag (pink), hemagglutinin (HA) tag (purple), myc tag (grey) and a PDGFR transmembrane domain (brown); GluBP 1-253 and 254-279 fragments are in light and dark blue, respectively;  $\Delta 8$  aa and  $\Delta 5$  aa specify deletions at the N- and C-terminus of GluBP introduced in GluSnFR. (b) Design of selected iGluSnFR variants. Crystal structure of GluBP (PDB 2VHA, adapted from (8)). Selected mutated residues around the glutamate site are shown as red and green backbone. Bound glutamate is represented in orange space filling display. (c) Equilibrium glutamate binding titrations at 20 °C for iGluSnFR (●), iGluSnFR E25D (iGlu<sub>f</sub>) (▼) and iGluSnFR S72T (iGlu<sub>u</sub>) (▲) *in vitro*; (d) Glutamate titrations *in situ* at 37 °C. iGluSnFR, iGlu<sub>f</sub> and iGlu<sub>u</sub> were expressed in HEK293T cells and titrated with glutamate. Data derived from iGluSnFR (n = 19), iGlu<sub>f</sub> (n = 41) and iGlu<sub>u</sub> (n = 33). (e) Representative images of HEK293T cells prior to glutamate addition and at saturating (1, 3 and 10 mM, respectively) glutamate. The scale bar represents 10  $\mu$ m. Glutamate dissociation kinetics of (f) iGluSnFR, (g) iGlu<sub>f</sub> and (h) iGlu<sub>u</sub> determined by stopped-flow fluorimetry. Experimental data (dotted lines) are overlaid by curves fitted to single exponentials (solid lines). Fluorescence changes are normalised to  $F_{max}$  of 1. Imaging glutamate release from single presynaptic terminals. (i) Schematic representation of hippocampal slice with transfected and patch-clamped CA3 pyramidal cell. (j) Spiral scan intersecting site of vesicular fusion. (k) Zoomed-in image of single trial iGlu<sub>u</sub> response. Decay time ( $\tau_{off}$ ) measurements with bleach correction (solid lines) for individual experiments by single exponential fit for (l) iGluSnFR (n = 13 boutons, 500 Hz sampling rate) and variants (m) iGlu<sub>f</sub> (n = 7 boutons, 1 kHz sampling rate) and (n) iGlu<sub>u</sub> (n = 7 boutons, 1 kHz sampling rate).

slice cultures of rat hippocampus, iGlu<sub>u</sub> directly reports discrete synaptic glutamate release events at 100 Hz. Combining high-speed two-photon imaging and electrophysiology, we show that short-term depression of Schaffer collateral AMPA responses is fully accounted for by the depression of glutamate release. Furthermore, we show a tight correlation between paired-pulse facilitation and rapid recovery from post-tetanic depression at individual boutons, suggesting that differential use of presynaptic resources (readily releasable vesicles) determines the filtering properties of CA3 pyramidal cell boutons.

## Results

**Affinity variants of iGluSnFR by binding site mutations.** We generated six iGluSnFR variants by mutating residues coordinating glutamate or in the vicinity of the binding site (9). Two of the mutations lowered, and four increased, the  $K_d$  for glutamate. Variants in order of increasing  $K_d$  were E25A < E25R < iGluSnFR < E25D < S72T < R24K < T92A (from 19  $\mu$ M to 12 mM) with Hill coefficients of 1.3 to 2.6 (SI Appendix Fig. S1a and Table S1).

We selected the two variants with the fastest response kinetics, iGluSnFR E25D (termed iGlu<sub>f</sub>) and iGluSnFR S72T (termed

iGlu<sub>u</sub>) (Fig. 1a,b) for detailed biophysical characterization as isolated proteins and as membrane-bound glutamate sensors on HEK293T cells and pyramidal neurons. Selectivity for glutamate was determined against aspartate, glutamine, D-serine, GABA and glycine. iGlu<sub>f</sub> and iGlu<sub>u</sub> affinities for aspartate were similar to that for glutamate, as previously reported for iGluSnFR (12), but with 2 to 3-fold lower fluorescence enhancement. The affinity for glutamine was in the mM range for all three probes (SI Appendix Fig. S1b, Table S3). D-serine, GABA and glycine evoked no detectable response.  $pK_a$  for the glutamate-bound form was  $\sim 6.5$  for iGluSnFR, iGlu<sub>f</sub> and iGlu<sub>u</sub>, whereas the apo-form showed little pH dependence indicating a well-shielded chromophore (SI Appendix Fig. S1c-e). Brightness values for iGlu<sub>f</sub> and iGlu<sub>u</sub> were similar to that for iGluSnFR (SI Appendix Table S2). *In vitro* measurements gave a dissociation constant ( $K_d$ ) for glutamate of 33  $\mu$ M for iGluSnFR, similar to that previously reported (12), while iGlu<sub>f</sub> and iGlu<sub>u</sub> had increased  $K_d$  values of 137  $\mu$ M and 600  $\mu$ M, respectively (Fig. 1c, SI Appendix Table S1). When expressed on the membrane of HEK293T cells,  $K_d$  values for glutamate were reduced to  $3.1 \pm 0.3$   $\mu$ M for iGluSnFR,  $26 \pm 2$   $\mu$ M for

273  
274  
275  
276  
277  
278  
279  
280  
281  
282  
283  
284  
285  
286  
287  
288  
289  
290  
291  
292  
293  
294  
295  
296  
297  
298  
299  
300  
301  
302  
303  
304  
305  
306  
307  
308  
309  
310  
311  
312  
313  
314  
315  
316  
317  
318  
319  
320  
321  
322  
323  
324  
325  
326  
327  
328  
329  
330  
331  
332  
333  
334  
335  
336  
337  
338  
339  
340

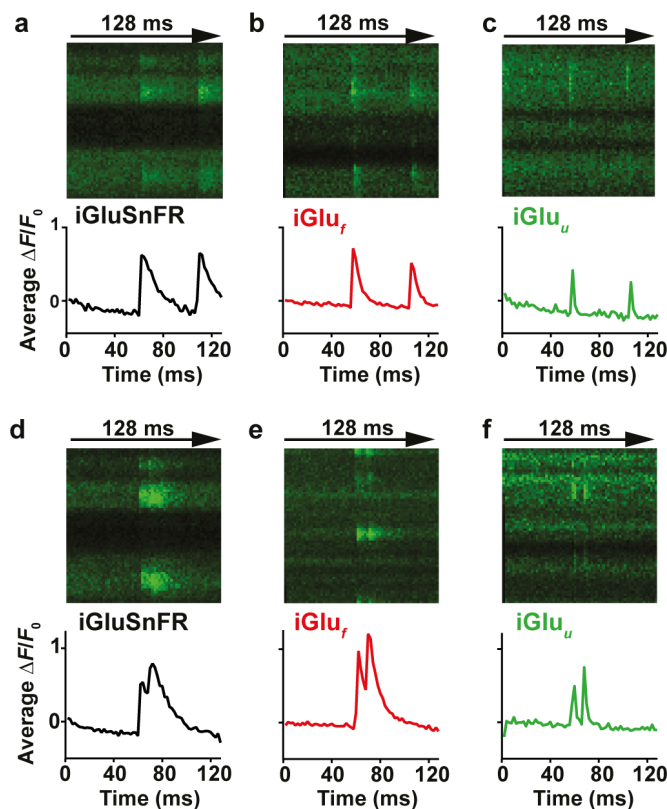


**Fig. 2.** Imaging glutamate release from single presynaptic terminals. Spiral line scans at 500 Hz were used to cover the entire surface of individual boutons, intersecting the release site multiple times. Averages of 3-6 responses of (a, d) iGluSnFR, (b, e) iGlu<sub>f</sub> and (c, f) iGlu<sub>u</sub>-expressing boutons stimulated by 2 somatic APs at 48 ms (a-c) and 10 ms inter-stimulus intervals (d-f).

iGlu<sub>f</sub> and  $53 \pm 4 \mu\text{M}$  for iGlu<sub>u</sub> (measured at 37 °C, **Fig. 1d,e**). A similar reduction of the  $K_d$  in the cellular environment compared to that in solution was reported for iGluSnFR (12). The *in situ* fluorescence dynamic range ( $F_{+Glu} - F_{-Glu}$ )/ $F_{-Glu}$  or  $\Delta F/F_0$  was  $1.0 \pm 0.1$  for both iGluSnFR and iGlu<sub>f</sub>, but 1.7-fold larger for iGlu<sub>u</sub>.

**Kinetic measurements of iGluSnFR variants *in vitro* and *in situ*.** Based on their large  $K_d$  values, we expected iGlu<sub>f</sub> and iGlu<sub>u</sub> to have faster glutamate release kinetics than iGluSnFR. Fluorescence measurements in a stopped-flow instrument indeed revealed faster *off*-rates for the new variants: using the non-fluorescent high-affinity GluBP 600n (10) in excess (0.67 mM) to trap released glutamate,  $k_{off}$  values of  $110 \text{ s}^{-1}$  ( $\tau_{off} = 9 \text{ ms}$ ),  $283 \text{ s}^{-1}$  ( $\tau_{off} = 4 \text{ ms}$ ) and  $468 \text{ s}^{-1}$  ( $\tau_{off} = 2 \text{ ms}$ ) were obtained for iGluSnFR, iGlu<sub>f</sub> and iGlu<sub>u</sub>, respectively, at 20 °C (**Fig. 1f-h** and **SI Appendix Table S4**). To compare *in vitro* response kinetics to physiological measurements, the temperature dependencies of the *off*-rates of iGluSnFR and the fast variants were determined. Linear Arrhenius plots were obtained between 4 °C and 34 °C (**SI Appendix Fig. S1f,g**). For the fast variants, values exceeding the temporal precision of our stopped-flow device were linearly extrapolated. At 34 °C, decay rates were  $233 \pm 3 \text{ s}^{-1}$  for iGluSnFR ( $\tau_{off} = 4.3 \text{ ms}$ ),  $478 \pm 5 \text{ s}^{-1}$  for iGlu<sub>f</sub> ( $\tau_{off} = 2.1 \text{ ms}$ ) and  $1481 \pm 74 \text{ s}^{-1}$  for iGlu<sub>u</sub> ( $\tau_{off} = 0.68 \text{ ms}$ ). Thus, we were able to improve iGluSnFR kinetics by a factor of 6.3.

To image glutamate dynamics in the synaptic cleft, we expressed the newly generated iGluSnFR variants in CA3 pyramidal cells in organotypic slice culture of rat hippocampus. Fluorescence was monitored at single Schaffer collateral terminals in CA1 by spiral scanning (**Fig. 1i,j**) while APs were triggered by brief (2 ms) depolarizing current injections into the soma of

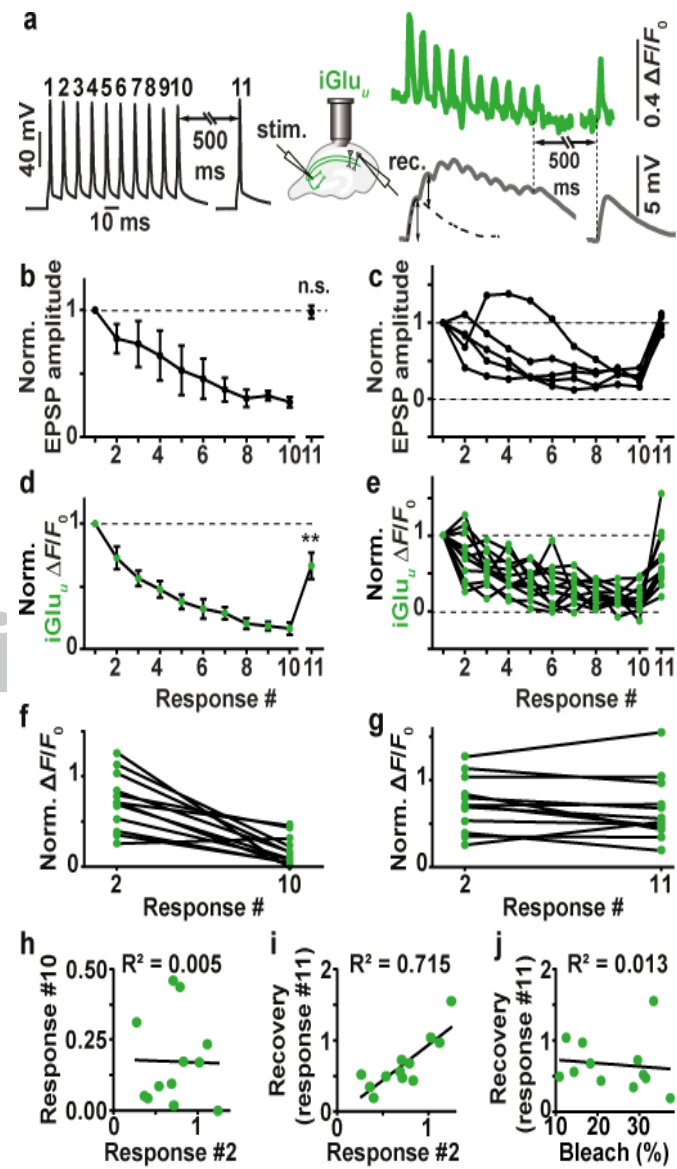


**Fig. 3.** Depression and recovery of synaptic transmission during 100 Hz trains. (a) Example of patch-clamp recording from a connected pair of CA3-CA1 pyramidal cells. Black trace: induced action potentials (APs) in CA1 pyramidal cell, 100 Hz train and single AP. Gray trace: EPSPs in CA1 pyramidal cell (average of 50 sweeps). The single AP response (right) was used to extract EPSP amplitudes from the burst response (dotted line). Green trace: average of 10 sweeps of single-bouton iGlu<sub>u</sub> responses to identical stimulation. (b) EPSPs (deconvoluted amplitudes) show strong depression during the 100 Hz train, followed by full recovery 500 ms later ( $n = 5$  CA3-CA1 pairs); two-tailed student's test comparing EPSP #1 and EPSP #11. (c) Individual paired recordings show consistent depression (response #10) and recovery (response #11). (d) Glutamate release shows strong depression during the 100 Hz train and partial recovery 500 ms later ( $n = 12$  boutons, 8 cells); two-tailed student's test comparing response #1 and response #11 ( $p$ -value: 0.0034). (e) Individual Schaffer collateral boutons show large variability in response #2 and in recovery response (#11) (f) responses by iGlu<sub>u</sub> to the second AP (paired-pulse facilitation/depression) were not correlated with total depression (response #10 normalized to response #1). (g) iGlu<sub>u</sub> responses to the second AP (response #2 normalized to response #1) were highly correlated with recovery after 500 ms (response #11 normalized to response #1). Recovery was independent of indicator bleach ( $F_{0, \text{response \#11}} / F_{0, \text{response \#1}}$ ).

the transfected CA3 neuron. A zoomed-in iGlu<sub>u</sub> example trace sampled at 1 kHz, the resolution used in all quantitative experiments with this indicator, is shown (**Fig. 1k**) along with a three-

341  
342  
343  
344  
345  
346  
347  
348  
349  
350  
351  
352  
353  
354  
355  
356  
357  
358  
359  
360  
361  
362  
363  
364  
365  
366  
367  
368  
369  
370  
371  
372  
373  
374  
375  
376  
377  
378  
379  
380  
381  
382  
383  
384  
385  
386  
387  
388  
389  
390  
391  
392  
393  
394  
395  
396  
397  
398  
399  
400  
401  
402  
403  
404  
405  
406  
407  
408

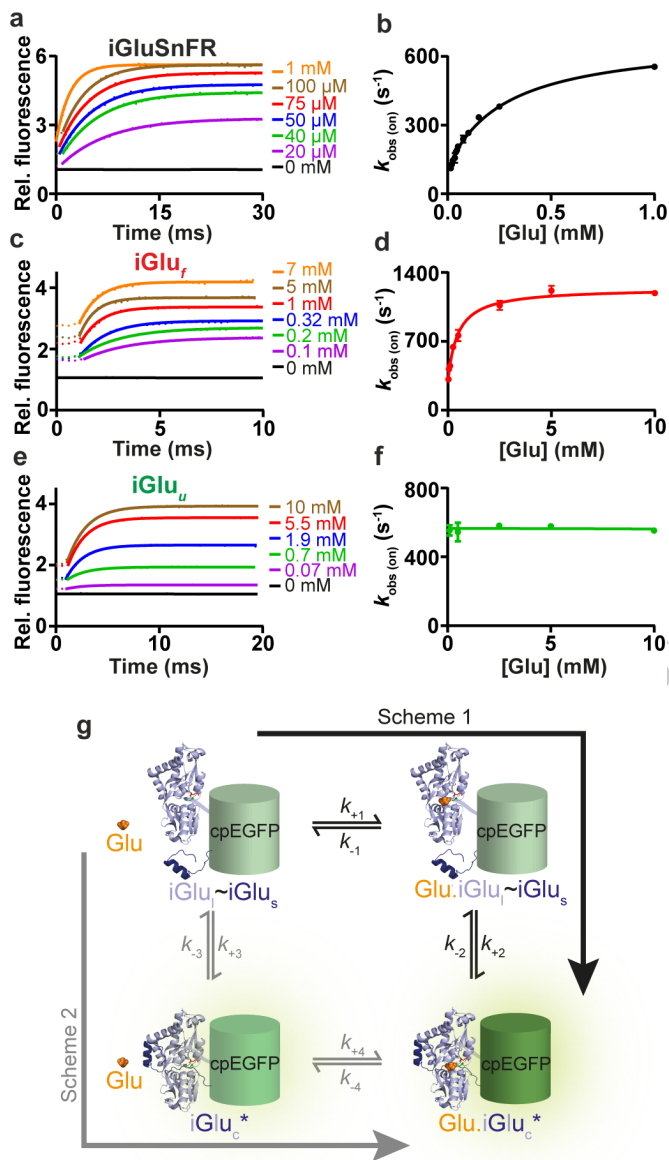


**Fig. 4.** Kinetics of glutamate binding by iGluSnFR variants (20 °C). (a, c, e) Glutamate association kinetics of iGluSnFR, iGlu<sub>f</sub> and iGlu<sub>u</sub>, respectively. Stopped-flow records of iGluSnFR, iGlu<sub>f</sub> and iGlu<sub>u</sub> reacting with the indicated concentrations of glutamate. Experimental data (dotted lines) are overlaid with curves fitted to single exponentials (solid lines); (b, d, f) Plot of observed association rates,  $k_{\text{obs(on)}}$  of iGluSnFR, iGlu<sub>f</sub> and iGlu<sub>u</sub> as a function of glutamate concentration; (g) Cartoon diagram depicting the putative molecular transitions of iGluSnFR and its fast variants to the fluorescent state. Key: cpEGFP (green), GluBP 1-253 (iGlu<sub>f</sub>) (light blue) and 254-279 (iGlu<sub>u</sub>) (dark blue) fragments, glutamate (orange).

dimensional schematic of the scanning method. The iGluSnFR response started  $4.5 \pm 1.6$  ms (mean  $\pm$  SD) after the peak of the somatic action potential, consistent with a short propagation delay between CA3 and CA1. Consistent with the stochastic nature of glutamate release, individual boutons showed different release probabilities (median  $p_r = 0.56$ , range 0.05 – 1.0). For kinetic analysis, boutons with high release probability and good separation between release failures and successes were selected (SI Appendix Fig. S2). The measured fluorescence decay time constants ( $\tau_{\text{off}}$ ) were  $13.8 \pm 3.8$  ms for iGluSnFR,  $5.2 \pm 2.0$  ms for iGlu<sub>f</sub>, and  $2.6 \pm 1.0$  ms for iGlu<sub>u</sub> (Fig. 11-n, SI Appendix Fig. S3). Thus, compared to iGluSnFR, synaptic responses detected

by iGlu<sub>u</sub> were revealed to be faster by a factor of 5.3. Interestingly, blocking glutamate uptake with TBOA (40  $\mu$ M) did not slow down the decay of iGlu<sub>u</sub> fluorescence (SI Appendix Fig. S4), suggesting that after sparse activation of Schaffer collateral synapses, glutamate is rapidly cleared from the synaptic cleft by diffusion, not by active transport. The situation may be different in highly active neuropil (12, 16).

*Synaptic glutamate dynamics during high frequency stimulation.* With decay kinetics of 1-2 ms, iGlu<sub>f</sub> and iGlu<sub>u</sub> are promising tools for direct tracking of synaptic glutamate during high frequency stimulation. The response of iGluSnFR, iGlu<sub>f</sub> and iGlu<sub>u</sub> to paired-pulse stimulation (Fig. 2 and SI Appendix Fig. S2) and to trains of 10 action potentials (APs) at 50, 67 and 100 Hz (SI Appendix Fig. S5) was tested. While the responses of iGluSnFR and iGlu<sub>f</sub> suggested build-up of glutamate during high frequency stimulation, iGlu<sub>u</sub> responses revealed that even at 100 Hz stimulation, glutamate was completely cleared from the synaptic cleft between action potentials (Fig. 2f, SI Appendix Fig. S5i). Interestingly, the amplitudes of synaptic fluorescence signals ( $\Delta F/F_0$ ) were similar for all three indicators, suggesting that the on-rate, not the overall affinity, determined the number of glutamate-bound indicator molecules in the synaptic cleft.

Excitatory postsynaptic potentials (EPSPs) in CA1 become strongly depressed during high-frequency stimulation (17). We were interested whether EPSP depression during 100 Hz stimulation could be fully accounted for by depression of glutamate release from presynaptic boutons. In paired recordings from connected CA3-CA1 pyramidal cells, we triggered APs in the CA3 cell by brief current injections while monitoring postsynaptic potentials (EPSPs) in the CA1 cell. The protocol consisted of a short high frequency burst (10 APs at 100 Hz) followed by a single AP 500 ms after the burst to probe recovery of synaptic function (18). We repeated the protocol up to 100 times at 0.1 Hz and averaged the recorded traces (Fig. 3a,b,c). As expected, connected CA3-CA1 pyramidal cell pairs showed strong depression during the high frequency train. The response to the recovery test pulse (#11) was not significantly different from the first EPSP in the train, indicating full recovery of synaptic function. To investigate depression and recovery of glutamate release, we evaluated iGlu<sub>u</sub> signals during identical stimulation (Fig. 3d,e). Due to the extremely fast kinetics of the indicator, deconvolution of the fluorescence time course was not necessary: we read the peak amplitudes during the 100 Hz train directly from the averaged fluorescence time course (average of 10 individual trials sampled at 1 kHz). Glutamate release decreased during the train with a time course that matched EPSP depression (Fig. 3d). This result points to a purely presynaptic origin of depression, which is consistent with AMPA receptors rapidly recovering from desensitization after each release event ( $\tau_{\text{recovery}} = 5$  ms (19)). However, glutamate release 500 ms after the tetanus was still significantly depressed (two-tailed student's test,  $p$ -value: 0.0034) while AMPA receptor currents were not. This discrepancy suggests that the response of AMPA receptors to cleft glutamate was in fact potentiated 500 ms after the high frequency train, compensating for the reduced output of Schaffer collateral boutons.

*Paired-pulse facilitation correlates with rapid recovery from depression.* The rapid kinetics of iGlu<sub>u</sub> allowed us to analyze frequency filtering at individual boutons. On the second AP, boutons showed a wide range of facilitated (3 out of 12 boutons) or depressed responses (9 out of 12 boutons, Fig. 3e). The response to the tenth AP was strongly depressed in all boutons (16% of response amplitude to first AP), with no correlation between the second and the tenth response ( $R^2 = 0.005$ , Fig. 3f,h). Interestingly, a highly significant correlation was observed between the response to the second AP and the recovery response 500 ms after the high frequency train ( $R^2 = 0.715$ , Fig. 3g,i). In contrast, we found no correlation between the amount of bleaching in individ-

545 ual experiments ( $F_0(\text{pre-11}^{\text{th}} \text{ pulse})/F_0(\text{pre-1}^{\text{st}} \text{ pulse})$ ) and the am- 546 plitude of the recovery response ( $(\Delta F/F_0)_{11^{\text{th}} \text{ pulse}}/(\Delta F/F_0)_{1^{\text{st}} \text{ pulse}}$ ), 547 indicating that poor recovery was not caused by excessive bleaching 548 or dilution of indicator molecules (Fig. 3j). Thus, synapses 549 that showed pronounced paired-pulse facilitation were also able 550 to recover rapidly from depression, both of which is indicative of 551 a low utilization of presynaptic resources (18). Such boutons are 552 optimized for the transmission of high-frequency activity (spike 553 bursts). In contrast, boutons that showed paired-pulse depression 554 were still depressed 500 ms after the high-frequency train. These 555 boutons act as low-pass filters: they preferentially transmit iso- 556 lated APs preceded by a silent period.

557 *Response kinetics of iGluSnFR and variants iGlu<sub>f</sub> and iGlu<sub>u</sub> are* 558 *based on the rate of structural change.* Finally, we investigated the 559 response mechanism of iGluSnFR and its fast variants using fluo- 560 rescence stopped-flow with millisecond time resolution. In associ- 561 ation kinetic experiments (20 °C), the fluorescence response rates 562 ( $k_{\text{obs}}$ ) showed hyperbolic glutamate concentration dependence, 563 approaching saturating rates of 643 s<sup>-1</sup> and 1240 s<sup>-1</sup> for iGluSnFR 564 and iGlu<sub>f</sub>, respectively (Fig. 4a-d). For iGlu<sub>u</sub>, in contrast,  $k_{\text{obs}}$  565 was found to be concentration-independent at 604 s<sup>-1</sup> (Fig. 4e,f). 566 We considered two different reaction pathways to explain our 567 kinetic data (Fig. 4g). iGluSnFR is represented as a complex of 568 the large fragment of the GluBP domain (GluBP 1-253, iGlu<sub>l</sub>), N- 569 terminally flanking cpEGFP and of the C-terminally fused small 570 GluBP fragment (GluBP 254-279, iGlu<sub>s</sub>). The term iGlu<sub>l</sub>~iGlu<sub>s</sub>, 571 indicates that the large GluBP fragment iGlu<sub>l</sub> and the small 572 fragment iGlu<sub>s</sub> are within one molecule, albeit separated by the 573 intersecting cpEGFP. In Scheme 1, the binding of glutamate to 574 iGlu<sub>l</sub> in iGlu<sub>l</sub>~iGlu<sub>s</sub> is the primary step (no change in fluo- 575 rescence). Glutamate binding is followed by a conformational 576 change induced by the reattachment of iGlu<sub>s</sub> to Glu-bound iGlu<sub>l</sub>, 577 resulting in the highly fluorescent Glu.iGlu<sub>c</sub>\* complex (rate lim- 578 iting step). According to Scheme 1, the hyperbolic dependence 579 of the observed rate  $k_{\text{obs}}$  on the glutamate concentration [Glu] 580 has the intercept of the y-axis at  $k_{-2}$  (see SI Appendix Kinetic 581 Theory, eq. 7). At low [Glu], the initial linear slope gives  $k_{+2}K_1$ . At 582 high [Glu],  $k_{\text{obs}}$  tends to  $k_{+2}+k_{-2}$ . Although  $k_{\text{obs}}$  for iGlu<sub>u</sub> appears 583 essentially concentration independent, its kinetics is consistent 584 with Scheme 1, with  $k_{+2}+k_{-2}$  having a similar value to  $k_{-2}$  (SI 585 Appendix Table S5).

586 In the alternative pathway (Scheme 2), the reattachment 587 of iGlu<sub>s</sub> to iGlu<sub>l</sub> occurs without prior binding of glutamate. 588 Therefore, iGlu<sub>l</sub>~iGlu<sub>s</sub> with the GluBP fragments separated and 589 complete GluBP domain (iGlu<sub>c</sub>\*) are in equilibrium. The con- 590 formational change that represents the reattachment of the two 591 GluBP fragments is expected to generate a fluorescent state of 592 cpEGFP. However, the equilibrium is likely to be strongly shifted 593 to the separated, non-fluorescent state (iGlu<sub>l</sub>~iGlu<sub>s</sub>). Assuming 594 that this equilibrium is fast and glutamate binding stabilizes the 595 fluorescent state, at low [Glu], a linear dependence of  $k_{\text{obs}}$  on 596 [Glu] is predicted with a slope of  $K_3k_{+4}/(1+K_3)$  and an intercept 597 of the y-axis at  $k_{-2}$  (see SI Appendix Kinetic Theory, eq. 15). 598 Although at low [Glu], mono-exponential fluorescence changes 599 are expected, as [Glu] increases, the concentration of iGlu<sub>c</sub>\* 600 cannot be assumed to be at steady-state and slow isomerisation 601 will limit  $k_{\text{obs}}$ , in a similar pattern to that for Scheme 1. Thus, 602 at high [Glu], even if iGlu<sub>c</sub>\* and Glu.iGlu<sub>c</sub>\* have equal relative 603 fluorescence intensities, biphasic fluorescence changes would be 604 expected for the association reactions. As all the reactions studied 605 here for the three variants had a single exponential appearance, 606 we can exclude Scheme 2 as a possible reaction pathway. In con- 607 clusion, Scheme 1 provides an excellent fit to our measurements 608 (SI Appendix Table S5), pointing to 'Venus fly-trap' closure by 609 glutamate binding as a required first step for the conformational 610 change that increases iGluSnFR fluorescence. 611 612

## Discussion

613 The development of iGluSnFR was a breakthrough in fluorescent 614 glutamate sensors towards investigating neurotransmission in liv- 615 ing organisms (20). Here we describe how to overcome one of the 616 key limitations of iGluSnFR, its slow response kinetics, and use 617 the new ultrafast variant iGlu<sub>u</sub> to investigate synaptic transmission 618 and frequency filtering at individual Schaffer collateral boutons. 619 For all tested variants, synaptic *off*-kinetics were slower by a 620 factor of 2.5 - 3.8 compared to temperature-matched *in vitro* mea- 621 surements on isolated protein. This is consistent with the much 622 higher affinities of HEK293T cell-expressed glutamate sensors 623 compared to soluble protein. These systematic differences, also 624 noted in the original characterization of iGluSnFR (12), may be 625 attributed to the tethering of the molecule to a membrane anchor, 626 slowing down conformational changes compared to free-floating 627 sensor molecules. Nevertheless, the relative differences in affinity 628 and kinetics of the new versions compared to iGluSnFR were 629 preserved *in vitro* and *in situ*. The *on*- and *off*-rates of iGlu<sub>u</sub> are 630 greater (2- and 5-6 fold, respectively) compared to iGluSnFR. 631 Interestingly, iGlu<sub>u</sub> was a faster reporter in the hippocampal slice 632 than iGlu<sub>f</sub>, even though the latter has a faster limiting *on*-rate. 633 iGlu<sub>u</sub> may be put at an advantage over iGlu<sub>f</sub> by its concentration- 634 independent response kinetics. It must be noted that the kinetics 635 of iGluSnFR-type indicators are ultimately limited by the struc- 636 tural change that reconstitutes the fluorescent complex, similar 637 to calcium-sensing GCaMPs. The constraints of the mechanism 638 with regard to the onset of fluorescence suggest that it cannot 639 be engineered to resolve sub-millisecond glutamate dynamics. 640 To achieve microsecond response times, it might be necessary to 641 develop hybrid glutamate indicators using synthetic dyes. 642 643

644 Synaptic iGlu<sub>u</sub> imaging revealed complete clearance of glu- 645 tamate between release events even at 100 Hz stimulation fre- 646 quency. The first attempts to estimate the time course of synaptic 647 glutamate transients were based on the decay of NMDA receptor 648 responses in primary cell culture: kinetic analysis of the dis- 649 placement of a competitive NMDA receptor antagonist suggested 650 glutamate clearance with  $\tau = 1.2$  ms (21). More recent studies 651 using computational modeling and fluorescence anisotropy imag- 652 ing in tissue suggest that it is closer to 100  $\mu$ s (22, 23). Thus, 653 due to the intrinsic kinetic limits of the iGluSnFR mechanism, 654 even iGlu<sub>u</sub> cannot resolve the true dynamics of free glutamate 655 in the synaptic cleft. Moreover, our spatiotemporal resolution is 656 limited by scanning, even though in most experiments, the spiral 657 scan line intersected the release site two or more times, and 658 thus effectively increased temporal sampling of cleft glutamate 659 by the same factor (e.g. from 1 to 2 kHz). In our analysis, we 660 binned all measurements (pixels) of a scan line into a single time 661 point (1 ms), potentially undersampling the sharp peak of iGlu<sub>u</sub> 662 signals (Fig. S6). For experiments where the peak amplitude of 663 iGlu<sub>u</sub> signals is of critical importance, temporal sampling could 664 be improved by assigning a time value to every pixel of the spiral 665 scan line before ROI analysis (Fig. S2). What we can say with 666 confidence is that accumulation of glutamate in the synaptic cleft 667 does not contribute to short-term plasticity at Schaffer collateral 668 synapses. 669

670 Glutamate release showed strong depression during 100 Hz 671 firing, in line with the expected depletion of release-ready ves- 672 cles. As we controlled the generation of every action potential 673 by somatic current injections, we can exclude decreased afferent 674 excitability as a source of depression in these experiments (17). 675 AMPA receptor currents during 100 Hz firing did not show more 676 run-down than iGlu<sub>u</sub> responses, suggesting that AMPA receptor 677 desensitization did not play a major role in the decrease of synap- 678 tic efficacy during the train. Paradoxically, AMPA responses were 679 fully recovered 500 ms after the train while the iGlu<sub>u</sub> response was 680 still significantly depressed. The most parsimonious explanation 681 is a long-lasting depression of glutamate release. There are al-

ternative scenarios that could explain smaller iGlu<sub>u</sub> responses on the 11<sup>th</sup> pulse, e.g. indicator molecules retrieved into endosomal structures during endocytosis, or accumulation of indicator in a (hypothetical) desensitized state. In these scenarios, facilitating boutons, which experience more exo- and endocytosis and iGlu<sub>u</sub> activation during the train, would be expected to show smaller responses at the 11<sup>th</sup> pulse. However, we found a strong correlation in the opposite direction, making these scenarios less likely.

As response amplitudes (40% - 120%  $\Delta F/F_0$ ) were typically less than half of the maximum change in fluorescence we determined for the three indicators (SI Appendix Table S3), we did not correct for the non-linearity of the iGluSnFR variants (Fig. 1c). To determine the absolute (or 'peak') glutamate concentration in the synaptic cleft, however, indicator saturation and undersampling would have to be taken into account.

The full recovery of the AMPA response points to an unexpected increase in sensitivity of the postsynaptic compartment to glutamate. By association with different auxiliary proteins and other scaffold-related mechanisms, the density and open probability of postsynaptic glutamate receptors can quickly change (24, 25). In hippocampal slice cultures, post-tetanic potentiation is well established and requires the activity of protein kinase C (26). Thus, it is possible that elevated Ca<sup>2+</sup> levels in the spine during our high frequency protocol enhanced AMPA receptor currents by a number of mechanisms, compensating for the reduced glutamate release 500 ms after the tetanus.

The surprisingly tight correlation between paired-pulse facilitation and rapid recovery from depression at individual boutons provides direct evidence that differential use of presynaptic resources determines the neural code between pyramidal cells (1, 18). Using Schaffer collateral synapses as an example, we show that iGlu<sub>u</sub> is a useful tool for a mechanistic analysis of high frequency synaptic transmission, interrogating presynaptic function independently of postsynaptic transmitter receptors.

## METHODS

1. Markram H, Wang Y, Tsodyks M (1998) Differential signaling via the same axon of neocortical pyramidal neurons. *Proc Natl Acad Sci U S A* 95:5323-5328.
2. Regehr WG (2012) Short-term presynaptic plasticity. *Cold Spring Harb Perspect Biol* 4:a005702.
3. Jenkins MA, Traynelis SF (2012) PKC phosphorylates GluA1-Ser831 to enhance AMPA receptor conductance. *Channels (Austin)* 6:60-64.
4. Best SL, Török K (2005) Development of a fluorescent glutamate binding protein. *Biophysical Journal* 88:464.
5. Chen GQ, Gouaux E (1997) Overexpression of a glutamate receptor (GluR2) ligand binding domain in *Escherichia coli*: application of a novel protein folding screen. *Proc Natl Acad Sci U S A* 94:13431-13436.
6. Kuusinen A, Arvola M, Keinänen K (1995) Molecular dissection of the agonist binding site of an AMPA receptor. *EMBO J* 14:6327-6332.
7. de Lorimier RM, Smith JJ, Dwyer MA, Looger LL, Sali KM, Paavola CD, Rizk SS, Sadigov S, Conrad DW, Loew L, Hellinga HW (2002) Construction of a fluorescent biosensor family. *Protein Sci* 11:2655-2675.
8. Hu Y, Fan CP, Fu G, Zhu D, Jin Q, Wang DC (2008) Crystal structure of a glutamate/aspartate binding protein complexed with a glutamate molecule: structural basis of ligand specificity at atomic resolution. *J Mol Biol* 382:99-111.
9. Hires SA, Zhu Y, Tsien RY (2008) Optical measurement of synaptic glutamate spillover and reuptake by linker optimized glutamate-sensitive fluorescent reporters. *Proc Natl Acad Sci U S A* 105:4411-4416.
10. Okumoto S, Looger LL, Micheva KD, Reimer RJ, Smith SJ, Frommer WB (2005) Detection of glutamate release from neurons by genetically encoded surface-displayed FRET nanosensors. *Proc Natl Acad Sci U S A* 102:8740-8745.
11. Tsien RY (2005) Building and breeding molecules to spy on cells and tumors. *FEBS Lett* 579:927-932.
12. Marvin JS, Borghuis BG, Tian L, Cichon J, Harnett MT, Akerboom J, Gordus A, Renninger SL, Chen TW, Bargmann CI, Orger MB, Schreiner ER, Demb JB, Gan WB, Hires SA, Looger LL (2013) An optimized fluorescent probe for visualizing glutamate neurotransmission. *Nat Methods* 10:162-170.
13. Nakai J, Ohkura M, Imoto K (2001) A high signal-to-noise Ca(2+) probe composed of a single green fluorescent protein. *Nat Biotechnol* 19:137-141.
14. Baird GS, Zacharias DA, Tsien RY (1999) Circular permutation and receptor insertion within green fluorescent proteins. *Proc Natl Acad Sci U S A* 96:11241-11246.
15. Taschenberger H, Woehler A, Neher E (2016) Superpriming of synaptic vesicles as a common

We provide a detailed description of the methods, data analysis and kinetic modeling in the online Supporting Information. Plasmids for iGlu<sub>r</sub>, iGlu<sub>u</sub> will be deposited at Addgene and made available once the manuscript is accepted for publication.

**Materials.** pCMV(MinDis), iGluSnFR and pRSET FLIPE-600n plasmids were a gift from Loren Looger (Addgene Plasmid #41732) and Wolf Frommer (Addgene plasmid # 13537), respectively. Site-directed mutagenesis was carried out following the QuikChange II XL protocol (Agilent Technologies).

**Fluorescence spectroscopies.** Glutamate association and dissociation kinetic experiments of iGluSnFR proteins were carried out on a Hi-Tech Scientific SF-61DX2 stopped-flow system equipped with a temperature manifold (27). Fluorescence spectra and equilibrium glutamate titrations were recorded on a Fluorolog3 (Horiba Scientific).

**In situ glutamate titration.** HEK293T cells were cultured on 24-well glass bottom plates in DMEM containing non-essential amino-acids (Life Technologies), 10% heat inactivated FBS (Life Technologies) and penicillin/streptomycin (100 U/mL, 100 mg/mL, respectively), at 37 °C in an atmosphere of 5% CO<sub>2</sub>. Cells were allowed 24 h to adhere before transfection with Lipofectamine 2000 (Invitrogen). Cells were examined at 37 °C (OKO lab incubation chamber) with a 3i Marianas spinning-disk confocal microscope equipped with a Zeiss AxioObserver Z1, a 40x/NA1.3 oil immersion objective and a 3i Laserstack as excitation light source (488 nm).

**Synaptic measurements.** Organotypic hippocampal slices (400 μm) were prepared from male Wistar rats at postnatal day 5 as described (28). iGluSnFR and variant plasmids were electroporated into 2-3 CA3 pyramidal cells at 40 ng/μL (iGluSnFR) or 50 ng/μL (iGlu<sub>r</sub>, iGlu<sub>u</sub>) together with tdimer2 (20 ng/μL), a cytoplasmic red fluorescent protein (29). 2 - 4 days after electroporation (at DIV 14-30), slice cultures were placed in the recording chamber of a two-photon microscope and superfused with artificial cerebrospinal fluid. Whole-cell recordings from a transfected CA3 pyramidal cell were made with a Multiclamp 700B amplifier (Molecular Devices). Red and green fluorescence was detected through the objective (LUMPLFN 60XW, 60x, NA 1.0, Olympus) and through the oil immersion condenser (NA 1.4, Olympus) using 2 pairs of photomultiplier tubes (H7422P-40SEL, Hamamatsu).

**Acknowledgements.** We thank Dr Zoltan Ujfalusi (University of Kent) for assistance with stopped-flow experiments, Iris Ohmert for the preparation of organotypic cultures and Dr David Trentham for comments on the manuscript. Use of The Institute of Translational Medicine, University of Liverpool Imaging Facility is gratefully acknowledged. This project was supported by the Wellcome Trust (Grant 094385/Z/10/Z to K.T.) and BBSRC (Grant BB/M02556X/1 to K.T.); the German Research Foundation (SPP 1665, SFB 936, FOR 2419 to T.G.O.; SPP 1926, FOR 2419 to J.S.W.) and the European Research Council (ERC-2016-StG 714762 to J.S.W.).

- basis for intersynapse variability and modulation of synaptic strength. *Proc Natl Acad Sci U S A* 113:E4548-E4557.
16. Zheng K, Rusakov DA (2015) Efficient integration of synaptic events by NMDA receptors in three-dimensional neuropil. *Biophys J* 108:2457-2464.
17. Kim E, Owen B, Holmes WR, Grover LM (2012) Decreased afferent excitability contributes to synaptic depression during high-frequency stimulation in hippocampal area CA1. *J Neurophysiol* 108:1965-1976.
18. Tsodyks MV, Markram H (1997) The neural code between neocortical pyramidal neurons depends on neurotransmitter release probability. *Proc Natl Acad Sci U S A* 94:719-723.
19. Crowley JJ, Carter AG, Regehr WG (2007) Fast vesicle replenishment and rapid recovery from desensitization at a single synaptic release site. *J Neurosci* 27:5448-5460.
20. Xie Y, Chan AW, McGirr A, Xue S, Xiao D, Zeng H, Murphy TH (2016) Resolution of High-Frequency Mesoscale Intracellular Maps Using the Genetically Encoded Glutamate Sensor iGluSnFR. *J Neurosci* 36:1261-1272.
21. Clements JD, Lester RA, Tong G, Jahr CE, Westbrook GL (1992) The time course of glutamate in the synaptic cleft. *Science* 258:1498-1501.
22. Scimemi A, Beato M (2009) Determining the neurotransmitter concentration profile at active synapses. *Mol Neurobiol* 40:289-306.
23. Zheng K, Jensen TP, Savtchenko LP, Levitt JA, Suhling K, Rusakov DA (2017) Nanoscale diffusion in the synaptic cleft and beyond measured with time-resolved fluorescence anisotropy imaging. *Sci Rep* 7:42022.
24. Compans B, Choquet D, Hossy E (2016) Review on the role of AMPA receptor nano-organization and dynamic in the properties of synaptic transmission. *Neurophotonics* 3:041811.
25. Carbone AL, Plested AJ (2016) Superactivation of AMPA receptors by auxiliary proteins. *Nat Commun* 7:10178.
26. Brager DH, Cai X, Thompson SM (2003) Activity-dependent activation of presynaptic protein kinase C mediates post-tetanic potentiation. *Nat Neurosci* 6:551-552.
27. Walklate J, Geeves MA (2015) Temperature manifold for a stopped-flow machine to allow measurements from -10 to +40 degrees C. *Anal Biochem* 476:11-16.
28. Gee CE, Ohmert I, Wiegert JS, Oertner TG (2017) Preparation of Slice Cultures from Rodent Hippocampus. *Cold Spring Harb Protoc* 2017(2):pdb.prot094888. doi: 10.1101/pdb.prot094888.
29. Wiegert JS, Gee CE, Oertner TG (2017) Single-Cell Electroporation of Neurons. *Cold Spring Harb Protoc* 2017(2):pdb.top089714. doi: 10.1101/pdb.top089714.